

## Article

# Stability Index of Surrounding Rock during Deep Rock Excavation Considering Energy Release Speed

Sheng Luo <sup>1,2</sup>, Peng Yan <sup>2,\*</sup>, Wenbo Lu <sup>2</sup> , Zhihong Dong <sup>1</sup>, Chunhua Zhou <sup>1</sup>, Zhaowei Yang <sup>1</sup> and Yingguo Hu <sup>1</sup>

<sup>1</sup> Key Laboratory of Geotechnical Mechanics and Engineering of Ministry of Water Resources, Changjiang River Scientific Research Institute, Wuhan 430010, China

<sup>2</sup> State Key Laboratory of Water Resources and Hydropower Engineering Science, Wuhan University, Wuhan 430072, China

\* Correspondence: pyanwhu@whu.edu.cn

**Abstract:** Rockburst is a kind of dynamic rock failure process that is easily induced by the excavation of a high-stress rock mass. However, from an energy perspective, the existing indexes for rockburst tendency have a limitation in that they do not consider the energy release speed. In this study, energy release effectiveness was proposed based on the local energy release rate while considering the influence of the energy release speed. The index can evaluate the stability of surrounding rock during the excavation of high-stress rock. The index can be obtained by recording the strain energy density of every element in the model during excavation and identifying the maximum strain energy density ( $E_{i\max}$ ), the minimum strain energy density ( $E_{i\min}$ ), the maximum time ( $t_{i\max}$ ), and the minimum time ( $t_{i\min}$ ) to calculate energy release speed and energy release effectiveness. A case study of the excavation of an experimental tunnel, namely, the URL of AECL, was adopted to validate the index. The results indicated that the proposed index can clearly identify the location and strength of the impact tendency area, and it can be effectively applied to the stability analysis during the excavation of deep tunnels.

**Keywords:** stability analysis; high in situ stress; rockburst; energy release speed; energy release effectiveness



**Citation:** Luo, S.; Yan, P.; Lu, W.; Dong, Z.; Zhou, C.; Yang, Z.; Hu, Y. Stability Index of Surrounding Rock during Deep Rock Excavation Considering Energy Release Speed. *Appl. Sci.* **2023**, *13*, 3000. <https://doi.org/10.3390/app13053000>

Academic Editor: Arcady Dyskin

Received: 9 February 2023

Revised: 22 February 2023

Accepted: 23 February 2023

Published: 26 February 2023



**Copyright:** © 2023 by the authors. Licensee MDPI, Basel, Switzerland. This article is an open access article distributed under the terms and conditions of the Creative Commons Attribution (CC BY) license (<https://creativecommons.org/licenses/by/4.0/>).

## 1. Introduction

Under the constraints of the United Nations Framework Convention on climate change and carbon emission rights, controlling carbon emissions has become a precondition and consensus of development all over the world. Hence, the development of alternative clean energy sources, such as hydropower, is of great significance to the energy structure. However, areas abundant in hydropower energy often have a significant elevation drop; due to the influence of topography, large-scale underground rock mass excavation is required [1]. As the burial depth increases, tectonic movement of the crust and rock stratum generates a tectonic stress field, which, when combined with the gravitational stress field, can result in extremely high in situ stress. For instance, the diversion tunnel of the Jinping II hydropower station has a burial depth of up to 2500 m [2], with a measured maximum principal stress of 42 MPa and a predicted maximum principal stress of 72 MPa by deduction. The excavation of high-stress rock mass can easily induce dynamic damage to the surrounding rock and even induce engineering disasters, such as rockburst [3,4]. The disasters induced by high-stress rock excavation, represented by rockburst, pose significant threats to the safety of workers and construction equipment [5–7]. Therefore, ensuring the stability of surrounding rock is crucial for the construction of deep engineering projects.

Rockburst can be classified into two types: “self-excitation” and “far-field stimulation”. “Self-excitation” refers to a type of rockburst that occurs when the stress state of surrounding rocks changes during excavation, resulting in a reduction in the energy storage limit of surrounding rocks. If the energy storage of surrounding rocks exceeds their energy

storage limit, the stored energy will be released suddenly, resulting in a rockburst. “Far-field stimulation” refers to a type of rockburst induced by dynamic disturbance from a distance, such as blasting vibration, microseism, or other rockburst events. This type of disturbance may break the original equilibrium state of the surrounding rock and enables it to accumulate kinetic energy [8]. It is evident that the energy release of surrounding rock induced by excavation is closely related to the stability of the surrounding rock in both the near and far fields [9].

Numerous researchers investigated the influence of the energy release of surrounding rocks on their stability. Cook et al. [10] were the first to discover that the sudden release of initial stress during rock excavation can cause over-relaxation of rock and generate stress waves in the rock mass. The analysis results of the dynamic response of surrounding rock under ideal conditions of excavation of a long tunnel by Carter et al. [11] show that the unloading of initial stress can induce vibration in the surrounding rock. The faster the unloading rate of rock is, the greater the amplitude of the induced dynamic tensile stress field is. Huang et al. [12] found that the unloading rate and dynamic disturbance have significant effects on the occurrence and scale of rockburst. The research of Lu et al. [13] and Yi et al. [14] also indicated that the unloading wave induced by the blasting excavation of rock mass under medium- or high-level in situ stress is a crucial factor that leads to the relaxation of surrounding rock. The higher the initial in situ stress, the greater the amplitude of the excavation load is and the stronger the vibration of surrounding rock induced by it. Lu et al. [15] and Yan [16] further studied the vibration induced by dynamic unloading of in situ stress and compared it with the vibration induced by a blasting load. The results show that while the in situ stress is at a medium or high level, the vibration induced by dynamic unloading may be larger than that induced by the blasting load and become the primary component of the vibration of surrounding rocks. From the perspective of energy, Su et al. [8] adopted the local energy release rate (LERR) index proposed by the energy difference before and after rock failure. Guo et al. [17], Di et al. [18], and Sanki [19] took the time factor into consideration, but the method adopted to determine the coefficient in the equation that describes the rockburst process is insufficient in theory and can only be obtained by experience. It is still impossible to describe the dynamic process of the system and the distribution of released energy in detail. However, it demonstrates the concept of the “rate” of energy change during the rock damage process, which is significant for the development of energy theory [20].

Various research was conducted to explore the stability of rock mass affected by the release speed of energy. For instance, Feng et al. [21] combined numerical simulation and statistical analysis of the seismic energy of a slope to verify that increasing excavation speed is detrimental to the stability of surrounding rocks and increases the energy level of the tremor. Fu et al. [22] emphasized that the process of energy release should be considered in the analysis process rather than just the total plastic zone volume or total energy release amount in a region, which may not necessarily indicate the worst stability. Large-scale SCTO (single-cleavage trapezoidal open) specimens were used by Lang et al. [23] to conduct impulse tests, and the results showed that the crack growth speed, dynamic fracture toughness, and energy release rate increased with the loading rate, while the delayed cracking time decreased. It can be seen that the process of energy release of rock has effects on the state of the rock mass, and the faster the energy release of the rock mass, the more unstable it becomes.

However, most of the research on energy release induced by excavation was focused on the stress unloading of original rocks, with the amplitude of unloading being considered the main factor influencing the stability of surrounding rocks. The research on the change in energy is related to the state before and after excavation or between different excavation stages. There was little research on the time factor of energy release of surrounding rocks during excavation.

In this study, an index that considers the energy release rate of surrounding rocks during the excavation of deep tunnels and its influence on the stability of the surrounding

rock mass was proposed. Through numerical analysis and validation with monitoring data from Canadian underground laboratory test tunnels, the index was shown to effectively indicate the location and strength of potential impact areas. The contribution of this study lies in the incorporation of energy release speed in the evaluation of rockburst tendency, providing a more comprehensive understanding of the stability of surrounding rocks during the excavation of high-stress rock.

## 2. Local Energy Release Effectiveness

### 2.1. Local Energy Release Rate

Rockburst is a result of the release of elastic strain energy stored in the rock mass, and its manifestation is rock failure. The strain energy release of brittle hard rock is extensive during the excavation of a deep rock mass. In the construction of hydropower projects in China, most of the rockburst induced by the excavation of a deep rock mass is strain-type rockburst, which is mainly in the form of local deformation or a small mass ejection. Most rockbursts are caused by the change in the stress state of the surrounding rock during excavation, leading to a reduction in the energy storage limit of the rock mass, as well as the accumulation and dissipation of the energy of the surrounding rock. When the energy exceeds the energy storage limit of the rock mass, the rock mass will be destroyed and the strain energy stored in the rock mass will be released. The energy released by the rock failure will lead to the failure of the adjacent rock mass. Furthermore, the failure of the rock mass and the release of energy will cause stress waves, which will become the trigger to break the equilibrium state of the rock mass in the far field. At present, there is insufficient research on the detailed energy release process during rockburst. However, it is widely accepted that energy release is the basic feature of rockburst, and the more energy released by the rock mass, the greater the tendency toward rockburst.

Based on the above consideration, Su et al. [8] developed the local energy release rate index and conducted a quantitative analysis of the intensity of rockburst. The index represents the energy released when the strain energy stored in the surrounding rock exceeds the energy storage limit. The strain energy density of the elements before and after the excavation of a rock mass can be obtained via a numerical method. The local energy release rate can be calculated using the change in strain energy density before and after the failure of each element, as shown in Equation (1):

$$LERR_i = U_{i\max} - U_{i\min} \quad (1)$$

where  $LERR_i$  represents the local energy release rate of the element numbered  $i$ ,  $U_{i\max}$  represents the peak value of elastic strain energy density before the brittle failure of element numbered  $i$ , and  $U_{i\min}$  is the residual value of elastic strain energy density after the brittle failure of element numbered  $i$ . The elastic strain energy density can be calculated using Equation (2):

$$U_i = \left[ \sigma_1^2 + \sigma_2^2 + \sigma_3^2 - 2\nu(\sigma_1\sigma_2 + \sigma_2\sigma_3 + \sigma_1\sigma_3) \right] / 2E_0 \quad (2)$$

where  $\sigma_1$ ,  $\sigma_2$ , and  $\sigma_3$  are the major, intermediate, and minor principal stresses;  $\nu$  is Poisson's ratio; and  $E_0$  is the elastic modulus of rock.

The local energy release rate index takes into account the influence of the stress path on the energy release of surrounding rock during excavation. It can reflect the energy release caused by excavation disturbance under complex stress states to a certain extent and demonstrate the potential intensity of rockburst. However, this index only accounts for the peak and residual values of energy in the energy evolution process of surrounding rock under excavation disturbance, and the detailed evolution process of energy from the peak to the residual value is not considered, that is, it does not consider the influence of the speed of energy release.

## 2.2. Effect of the Energy Release Speed on the Energy Release Effectiveness

In the local energy release rate index described above, rock failure occurs when the accumulated energy in the surrounding rock exceeds its energy storage limit, and the released energy is considered the energy source for the rock mass nearby. The stability of a rock mass with high energy will be destroyed by an energy fluctuation, and the interlocking failure process can lead to rockburst. However, the energy release of rock alone is not enough to reflect the effectiveness of the energy release of the surrounding rock.

From a modern ballistics perspective, the effectiveness of a kinetic energy projectile on the target is determined by several factors: (1) the kinetic energy when the projectile hits the target, (2) the ability of the projectile to transmit energy to the target, (3) the area of energy transfer, (4) the speed of energy transfer, and (5) the effect of the shock wave induced by the projectile upon impact. While the first factor emphasizes the energy of the projectile, the second to fourth factors emphasize the process of energy transfer from the projectile to the target. It is clear that the kinetic energy of the projectile is a necessary but not sufficient condition for killing effectiveness. Assuming that the energy transferability of energy from the projectile to the target is poor, and it is difficult to ensure the effective transmission of the projectile energy to the target, the killing effectiveness of the projectile will be reduced or even ineffective. Therefore, in the design process, it is necessary to consider both the energy of the projectile itself and the process of its energy transfer to the target [24].

Explosions provide another example. From the perspective of energy, industrial explosives have relatively low energy density compared with common combustibles, such as coal (Table 1). The reaction heat of TNT, known as the “king of explosives”, is less than half of that of coal, and the reaction heat of black powder, used for gunpowder, is less than one-third of that of coal. The reaction heat of fulminating mercury and lead azide, which is still used for initiating explosives, is less than one-quarter of that of coal. However, coal cannot be used as an explosive because the reaction of general combustibles, such as coal, is very slow during the combustion process, and the energy release speed is very slow, whereas explosive reactions are rapid, and the energy release speed is very high. These examples illustrate that the energy release speed has a significant impact on the effectiveness of energy release.

**Table 1.** Comparison between the reaction heat of coal and some explosive substances.

Name of Combustible	Reaction Heat (kJ/kg)
Coal	8960
Nitroglycerin	6217
Nitrocotton	4291
Trinitrotoluene (TNT)	4187
Black powder	2784
Ammonium nitrate	4228
Fulminating mercury	1733
Lead azide	1536

## 2.3. Energy Release Effectiveness

Under the conditions above, combined with the local energy release rate index proposed by Su et al. [8], this study proposed a new index, that is local energy release effectiveness. The index considers both the energy released by the rock mass per unit volume and the energy released speed when the strain energy accumulated in the surrounding rock exceeds the energy storage limit of the rock mass. It is a quantitative index that can reflect the rockburst location and strength.

Based on the above considerations, the following steps can be used to obtain the local energy release effectiveness index through numerical simulation: Use a constitutive model that reflects the brittleness of the rock mass in the simulation. The strain energy density of every element in the model during the excavation process is recorded by custom variables defined with the Fish language. Then, the maximum strain energy density ( $E_{i\max}$ ),

the minimum strain energy density ( $E_{i\min}$ ), the maximum time ( $t_{i\max}$ ), and the minimum time ( $t_{i\min}$ ) are identified. The local energy release rate ( $LERR$ ) can be calculated with Equation (3):

$$LERR_i = E_{i\max} - E_{i\min} \quad (3)$$

The local energy release speed ( $LERS$ ) can be calculated with Equation (4):

$$LERS_i = \frac{E_{i\max} - E_{i\min}}{t_{i\min} - t_{i\max}} \quad (4)$$

The local energy release effectiveness ( $LERE$ ) can be calculated with Equation (5):

$$LERE_i = (E_{i\max} - E_{i\min}) \times f(LERS_i) \quad (5)$$

In Equation (5), there is no theoretical support for the relationship between the energy release speed and energy release effectiveness. Therefore, for the expression of  $f(LERS)$ , this study drew lessons from the relationship between the average fragment size of rock after blasting and the explosive intensity. The explosive intensity is closely related to its ability to crush and destroy the objects in contact with it during the explosion, which is the embodiment of its instantaneous power, and the fragment size of rock can reflect the crack growth density of rock to a certain extent. The specific description is interpreted as follows.

Sandia National Laboratory of the United States carried out experiments to study the relationship between the average fragment size of rock dynamic crushing and the loading rate, the relationship is shown in Equation (6):

$$d = \left( \frac{\sqrt{20}K_{Ic}}{\rho c \dot{\epsilon}} \right)^{2/3} \quad (6)$$

where  $d$  is the fragment size,  $K_{Ic}$  is the fracture toughness,  $\rho$  is the density,  $c$  is the elastic wave velocity, and  $\dot{\epsilon}$  is the strain rate of loading.

According to the research results of Li et al. [25], the rock strength under different loading rates can be approximately expressed as Equation (7):

$$\hat{\sigma} = k\dot{\epsilon}^{1/3} \quad (7)$$

where  $\hat{\sigma}$  is the strength of the rock and  $k$  is the coefficient related to the rock properties.

Substituting Equation (7) to Equation (6), the relationship between  $d$  and  $\sigma$  can be obtained, as shown in Equation (8):

$$d = \left( \frac{\sqrt{20}K_{Ic}}{\rho c \dot{\epsilon}} \right)^{2/3} \left( \frac{k}{\hat{\sigma}} \right)^2 \quad (8)$$

Furthermore, under the condition of rock blasting excavation, the cartridge in the blast hole will excite the stress wave after initiation, and the additional stress caused by the stress wave passing to the surrounding rock can be calculated with Equations (9) and (10):

$$\sigma = p_0 \left( \frac{r}{r_b} \right)^{-a} \quad (9)$$

$$p_0 = \frac{\rho_e D^2}{8} \left( \frac{V_c}{V_b} \right)^\gamma \quad (10)$$

where  $\sigma$  is the additional compressive stress induced by the detonation wave transfer into the rock mass,  $p_0$  is the blasting load applied to the borehole,  $r$  is the distance from the calculation point to the charge center,  $a$  is the attenuation index of the stress wave spreading in the rock,  $r_b$  is the radius of the borehole,  $\rho_e$  is the density of the explosive,  $D$  is the

explosive detonation velocity,  $V_b$  is the borehole volume, and  $V_c$  is the charge volume.  $\gamma$  is the pressure attenuation index of explosive product expansion; when the pressure in the borehole is greater than or equal to 100 MPa,  $\gamma = 3$ , and when the pressure in the borehole is less than 100 MPa,  $\gamma = 1.4$ .

Taking  $\sigma = \hat{\sigma}$ , and substituting Equations (7) and (8) into Equation (6), the result is Equation (11):

$$d = Ak^2(BD^2)^{-2} \tag{11}$$

The  $A$  and  $B$  in Equation (11) can be calculated with Equations (12) and (13):

$$A = \left( \frac{\sqrt{20}K_{Ic}}{\rho c} \right)^{2/3} \tag{12}$$

$$B = \rho_e \left( \frac{V_c}{V_b} \right)^\gamma \left( \frac{r}{r_b} \right)^{-a/8} \tag{13}$$

Therefore, the relationship between the explosive detonation velocity and rock fragmentation is as shown in Equation (14):

$$d \propto D^{-4} \tag{14}$$

Explosive detonation can destroy the surrounding rock, which is due to the direct and strong effect of high temperature and high-pressure detonation products. The greater the pressure of the detonation product, the greater the damage to the surrounding rock. Therefore, the detonation pressure of the condensed explosive can be used to represent the explosive's intensity. Furthermore, the explosive pressure can be calculated with Equation (15), and thus, the relationship between the explosive's intensity and detonation speed of the explosive will be Equation (16):

$$p_0 = \frac{1}{4}\rho_0 D^2 \tag{15}$$

$$IN \propto D^2 \tag{16}$$

where  $p_0$  is the explosive pressure of the explosive,  $\rho_0$  is the density of the explosive,  $D$  is the detonation speed of the explosive, and  $IN$  is the explosive's intensity.

$$d \propto IN^{-2} \tag{17}$$

Because a smaller fragment size means a smaller rock mass and more fragmentation, it can be considered that the fragmentation effect of rock is related to the square of the release speed of explosive energy. In view of this, the relationship between the energy release speed and energy release effectiveness was taken as Equation (18) in this study:

$$f(LERS) = LERS^2 \tag{18}$$

Therefore, the specific expression for the local energy release effectiveness in this study is shown in Equation (19):

$$LERE_i = LERR_i \times LERS_i^2 \tag{19}$$

### 3. Engineering Example

#### 3.1. Engineering Background

The deep geological disposal method is widely used for nuclear waste disposal and is adopted by most countries with nuclear power. In Canada, the plutonic rocks stratum in the depth range of 500 m to 1000 m of the Canadian Shield is selected as the underground space for settlement. To support this, the Canadian Atomic Energy Corporation (AECL)

built an Underground Research Laboratory (URL) for ‘Mine-by’ research on the Lac du Bonnet granite foundation. The site is located about 120 km north of Winnipeg, Manitoba. The first stage of the study involved excavating a tunnel to analyze the progressive failure process and the development of excavation-induced damage around the tunnel. The tunnel was excavated using a non-blasting method at the depth of 420 m, with a length of 46 m and a diameter of 3.5 m. During the excavation, brittle spalling failure of the tunnel wall continued to occur and developed into a typical ‘V-shaped’ rockburst pit. Taking the Lac du Bonnet granite at a location of 18 + 50m as an example, the final depth of the rockburst pit was about 1.3 times the radius of the tunnel. As shown in Figure 1, the failure area was almost symmetrical. However, due to the presence of waste rock and residue soil on the tunnel’s bottom plate during excavation, their weight caused a slight difference in the distribution of the failure area at the bottom and top of the tunnel. For the rock mechanics parameters, experiments had been conducted by the Canadian Centre for Minerals and Energy Technology (CANMET), and the rock mechanics test results for the rock at the site are shown in Table 2.

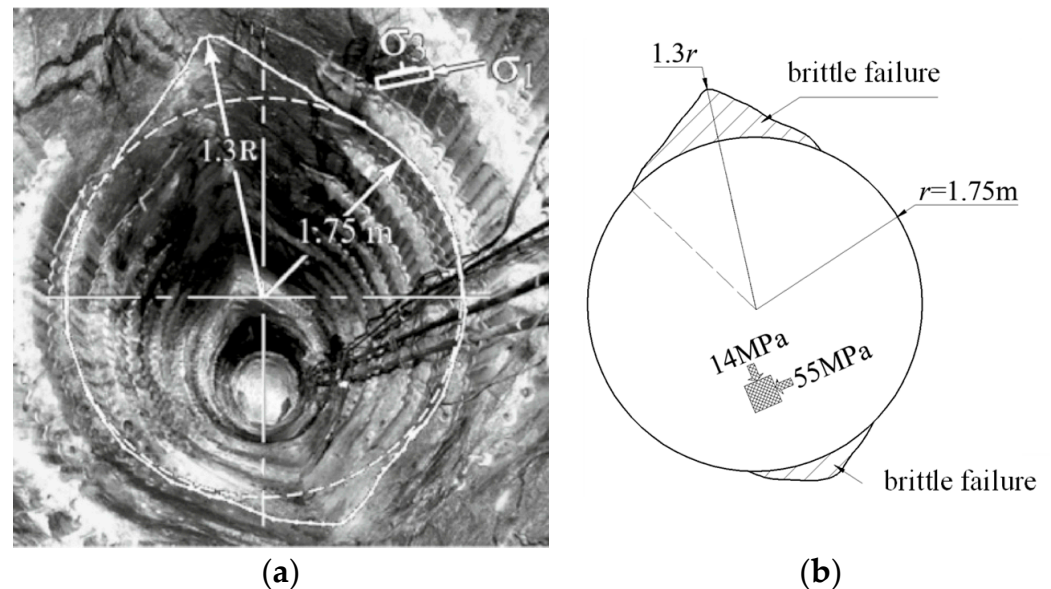


**Figure 1.** The final shape of the brittle failure of the test tunnel: (a) photograph [26,27]; (b) outline.

**Table 2.** Rock mechanics parameters provided by CANMET.

Rock Types	Granite	Granodiorite
Density ( $\text{kg}/\text{m}^3$ )	$2630 \pm 10$	$2660 \pm 10$
Uniaxial compressive strength (MPa)	$213 \pm 20$	$228 \pm 20$
Young’s modulus (GPa)	$65 \pm 5$	$66 \pm 5$
Poisson’s ratio	$0.25 \pm 0.05$	$0.25 \pm 0.05$

### 3.2. Engineering Background

In order to illustrate the applicability of the energy release effectiveness index intuitively, FLAC3D software was adopted to simulate the energy evolution process of the surrounding rock during the excavation of the mine by a test tunnel of the URL. The model, shown in Figure 2, had a size of  $30 \text{ m} \times 30 \text{ m}$  and an excavation radius of 1.75 m. To meet the calculation schedule, the minimum size of the model was 0.13 m and the maximum size was 1.67 m. The simulation utilized the cohesion-weakening–friction-strengthening model (CWFS), which is a variant of the strain-softening model. Its basic parameters are shown in Table 3, and the variation of cohesion and friction are shown in Table 4.

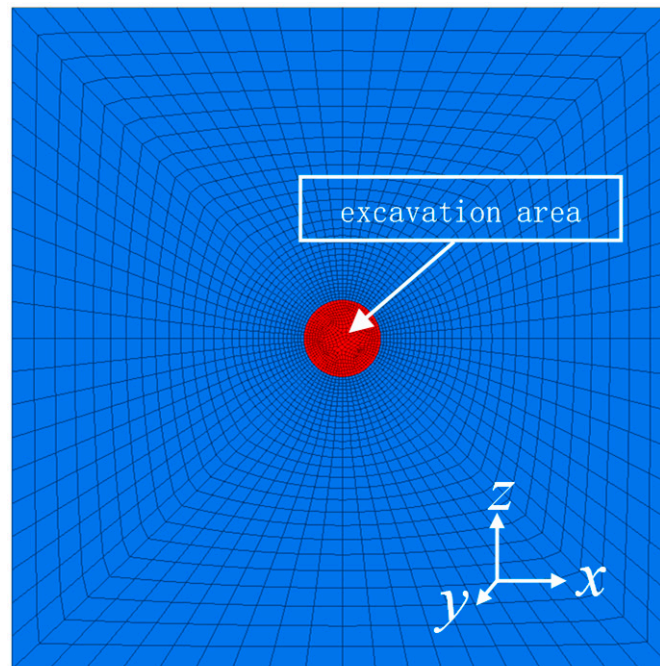


Figure 2. Numerical simulation model.

Table 3. Rock mass parameters of Lac Du Bonnet granite in the mine-by test tunnel.

Elastic Modulus	Poisson's Ratio	Compressive Strength	Density	Cohesion	Internal Friction Angle	Tensile Strength
60 GPa	0.25	120 MPa	2630 kg/m <sup>3</sup>	1.5 MPa	40°	10 MPa

Table 4. Variation of the cohesion and friction.

Initial Cohesion	Minimum Cohesion	Initial Internal Friction Angle	Maximum Internal Friction Angle
50 MPa	1.5 MPa	0°	40°

### 3.3. Boundary Condition

The in situ stress at an elevation of 420 m is shown in Table 5. We set  $\sigma_1$  to 55 MPa with an inclination angle of 10°. We set  $\sigma_3$  to 14 MPa and perpendicular to  $\sigma_1$  in the vertical plane. We set  $\sigma_2$  to 48 MPa and perpendicular to the plane  $\sigma_1 - \sigma_2$ . The details are shown in Figure 3.

Table 5. In situ stress at elevation 420.

Stress Component	$\sigma_1$	$\sigma_2$	$\sigma_3$
Value (MPa)	55 ± 5	48 ± 5	14 ± 1
Trend (°)	135 ± 10	44 ± 10	280 ± 25
Dip angle (°)	10 ± 5	5 ± 5	79 ± 5

The numerical model was established, where the horizontal direction of the tunnel was the x-axis, the vertical direction was the z-axis, and the axial direction was the y-axis. The measured maximum principal stress of the tunnel section had an angle of 10 degrees with the x-axis, the minimum principal stress had an angle of 10 degrees with the z-axis, and the intermediate principal stress was concentric with the y-axis. Assuming that  $\beta_{ij}$  was the projection of the i direction unit vector in the direction of j, then the matrix representing

the projection of the unit vector in the direction of  $x$ ,  $y$ , and  $z$  in the direction of the first, second, and third principal stresses could be expressed as Equation (20):

$$[\beta] = \begin{bmatrix} \beta_{x1} & \beta_{x2} & \beta_{x3} \\ \beta_{y1} & \beta_{y2} & \beta_{y3} \\ \beta_{z1} & \beta_{z2} & \beta_{z3} \end{bmatrix} = \begin{bmatrix} \cos 10 & 0 & -\sin 10 \\ 0 & 1 & 0 \\ \sin 10 & 0 & \cos 10 \end{bmatrix} \quad (20)$$

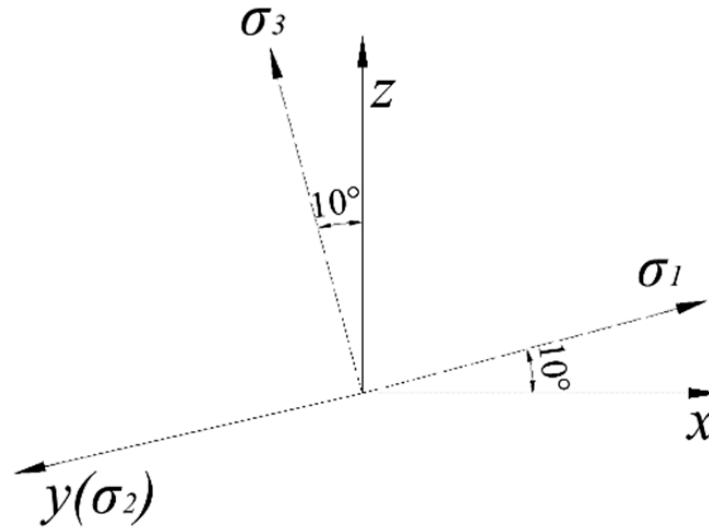


Figure 3. Direction of the stress.

After transforming the principal stress into three directions  $x$ ,  $y$ , and  $z$  as shown in Equation (21), the boundary conditions of the numerical model are shown in Figure 4.

$$[\sigma_{ij}] = [\beta][\sigma_{ij}][\beta]^T = \begin{bmatrix} 53.8 & 0 & 7.0 \\ 0 & 48 & 0 \\ 7.0 & 0 & 15.2 \end{bmatrix} \quad (21)$$

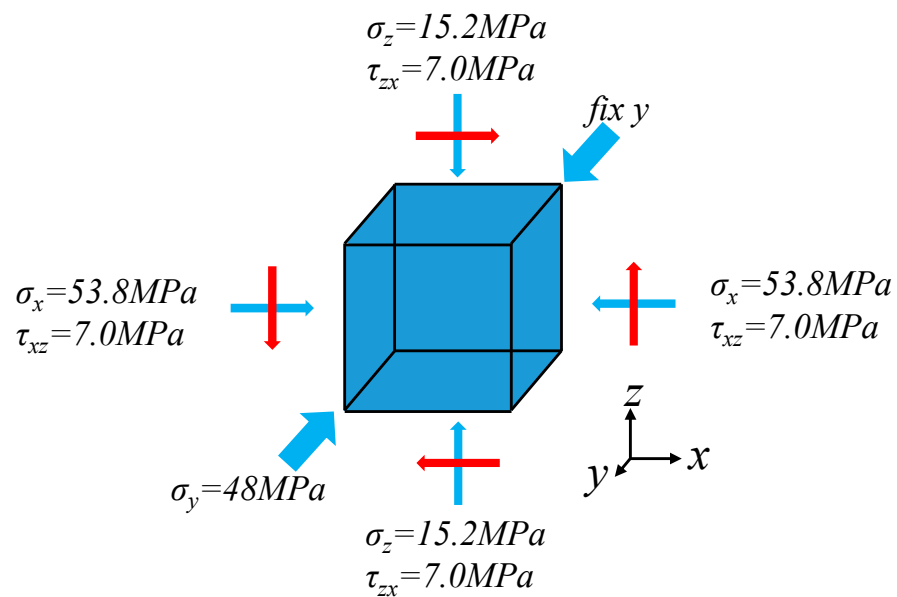


Figure 4. Boundary conditions of the numerical model.

#### 4. Results and Discussing

Stress balancing was performed before the excavation, and all units' strain energy densities were recorded at every iterative step using a customized variable. The variation process of the energy density of the maximum and minimum principal stress direction depths of 0 m, 0.2 m, 0.5 m, 1 m, 2 m, and 5 m with the simulation process is shown in Figure 5. It can be seen from the figure that stress release occurred in the unit in the direction of maximum principal stress at the moment of excavation due to the change in the stress state. Although some of the energy was restored during the subsequent stress adjustment, the final value was still less than the initial value. The energy release of the unit in the direction of the maximum principal stress occurred earlier, when the step was about 500, the energy release began at the measuring point buried 5 m, and the earlier the energy release occurred, the shallower the measuring point was buried. It can be seen that the change in stress state caused by the excavation induced the release of energy in the direction of minimum principal stress due to the unloading wave transmitted from the excavation to the depth of rock mass. The energy disturbance caused by the transient stress state change caused by the excavation of the unit in the direction of minimum principal stress could be neglected, and the whole process lasted less than 100 steps. Then, the energy rapidly accumulated during the stress redistribution process, with unit energy near the excavation boundary accumulating faster. When the strain energy accumulated to a certain extent, the unit was destroyed, and a portion of the strain energy was released.

The numerical results showed that the maximum strain energy density of the unit on the excavation boundary in the direction of large principal stress was  $29,059 \text{ J/m}^3$ , occurring before the 100th step (the excavation moment was the 100th step). The strain energy density after the energy release was  $8499 \text{ J/m}^3$  and it occurred at the 115th step. It can be seen from Figure 5a that the energy release in the direction of maximum principal stress occurred at the moment of excavation. The reason was that the stress state of the surrounding rock changed from three-direction compression to two-direction compression. The main factor was not the failure of the rock mass. Moreover, as the buried depth of the measuring point increased, the energy release process became smoother and the local energy release rate showed a decreasing trend.

From Figure 5b, it can be seen that the strain energy density of surrounding rocks in the direction of minimum principal stress was released after the process of accumulation after excavation. The maximum strain energy density on the excavation boundary in the direction of minimum principal stress was  $83,708 \text{ J/m}^3$ , occurring in the 839th step. After the energy release, the strain energy density was reduced to  $5594 \text{ J/m}^3$ , occurring in the 1081st step. The local energy release rate was  $78,114 \text{ J/m}^3$  and the energy release speed was  $323 \text{ J/m}^3$  per step, resulting in an energy release effectiveness of  $25.2 \times 10^6 \text{ J}^2/(\text{m}^6 \cdot \text{step})$ . For the element buried 0.2 m in the direction of minimum principal stress, the maximum strain energy density was  $123,482 \text{ J/m}^3$ , occurring in the 1191st step. After energy release, the strain energy density was reduced to  $3477 \text{ J/m}^3$ , occurring in the 2465th step. The local energy release rate was  $8705 \text{ J/m}^3$ , the energy release speed was  $70 \text{ J}/(\text{m}^3 \cdot \text{step})$ , and the energy release effectiveness was  $6.2 \times 10^6 \text{ J}^2/(\text{m}^6 \cdot \text{step})$ . Although the local energy release rate of the element at the excavation face was smaller than that of the 0.2 m buried depth, the energy release effectiveness was higher at the excavation face. As rockburst or a spalling rib often develops from the surface to the interior, these have certain advantages when it comes to using energy release effectiveness to evaluate the tendency of rock burst.

The maximum energy density before the energy release and the energy density after the energy release, as well as their occurrence time, are shown in Figures 6 and 7. It is apparent that there was significant energy accumulation in the direction of the minimum principal stress, and the peak energy occurred earlier on the excavation surface than in the rock mass. The distribution pattern of the energy density after release was similar to the maximum density, except that the low energy area appeared near the excavation surface.

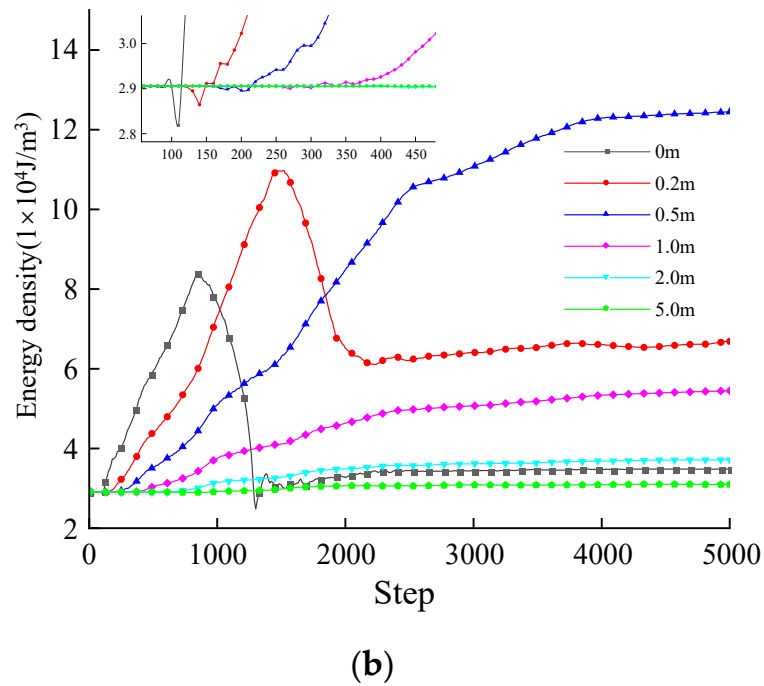
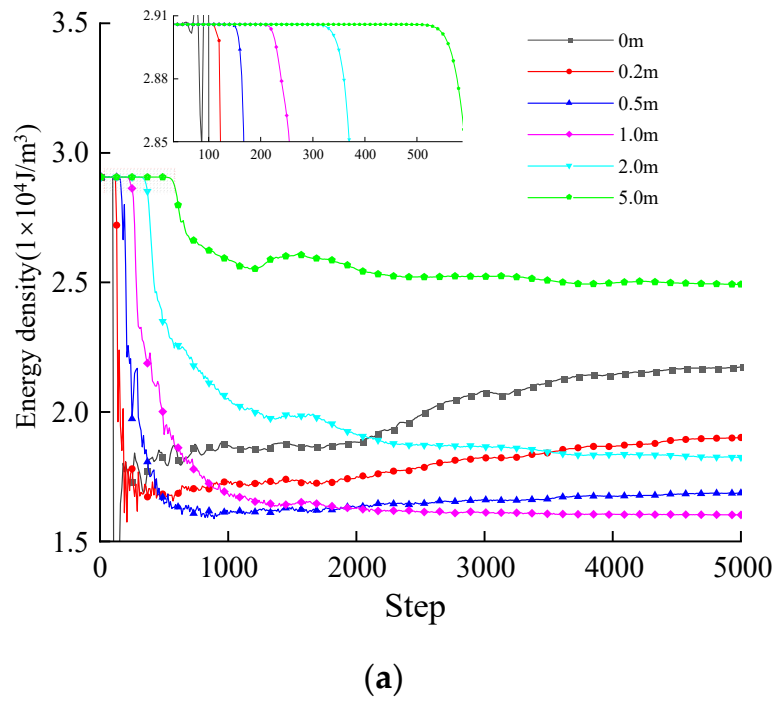
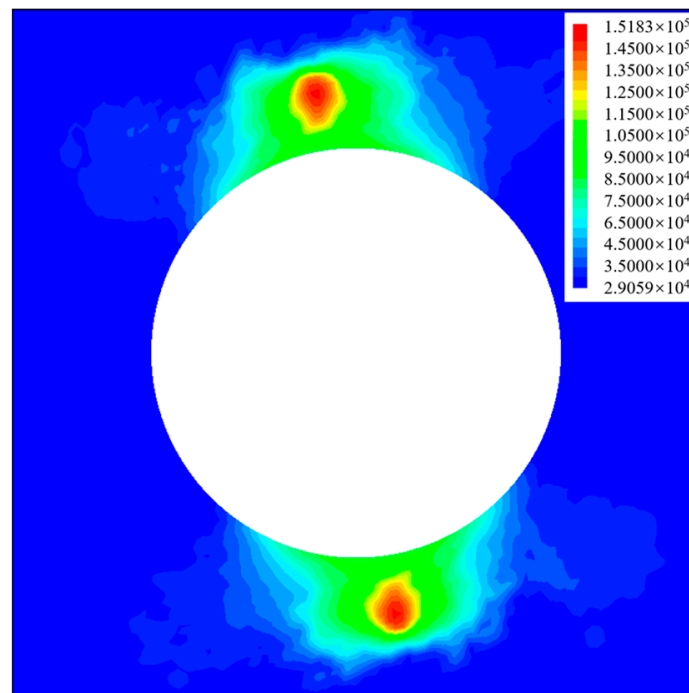
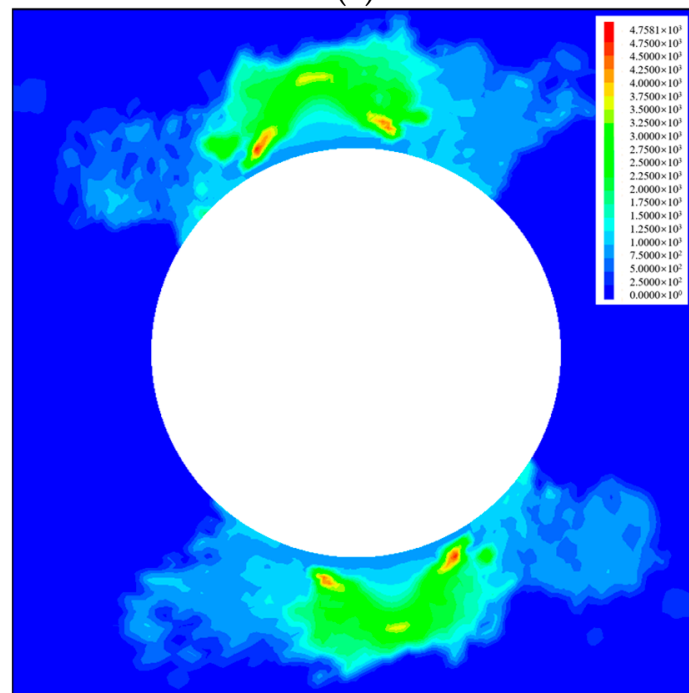


**Figure 5.** Energy path of elements at different depths of the tunnel wall: (a) measuring point in the maximum principal stress direction; (b) measuring point in the minimum principal stress direction.

The local energy release effectiveness (shown in Figure 8) could be calculated with the maximum energy density before and after the energy release, as well as their occurrence time. Taking one-tenth of the maximum value as the lower limit of the contour plot, it can be observed that the distribution of local energy release effectiveness aligned with the actual location of the rockburst well. The maximum radius was between 2.20 and 2.257 m, which was approximately 1.26–1.29 times the radius of the excavation zone, which closely matches the actual radius of 1.3 times.

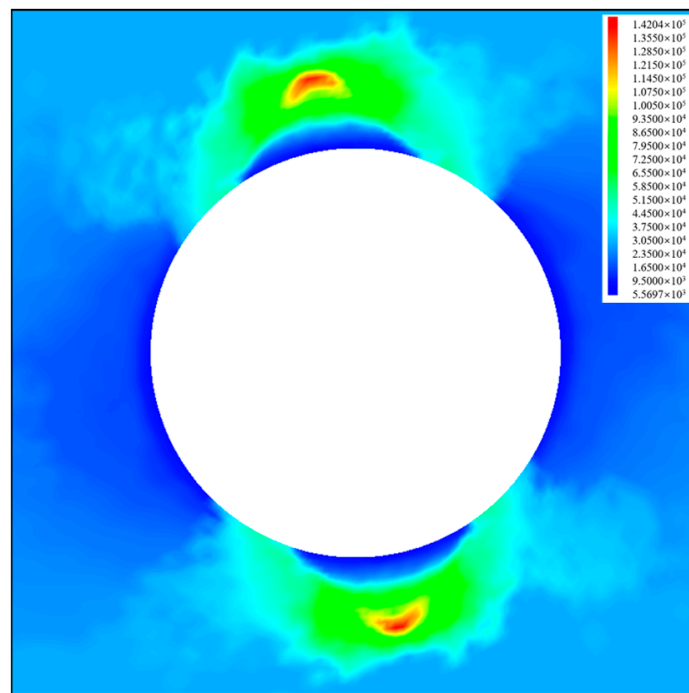


(a)

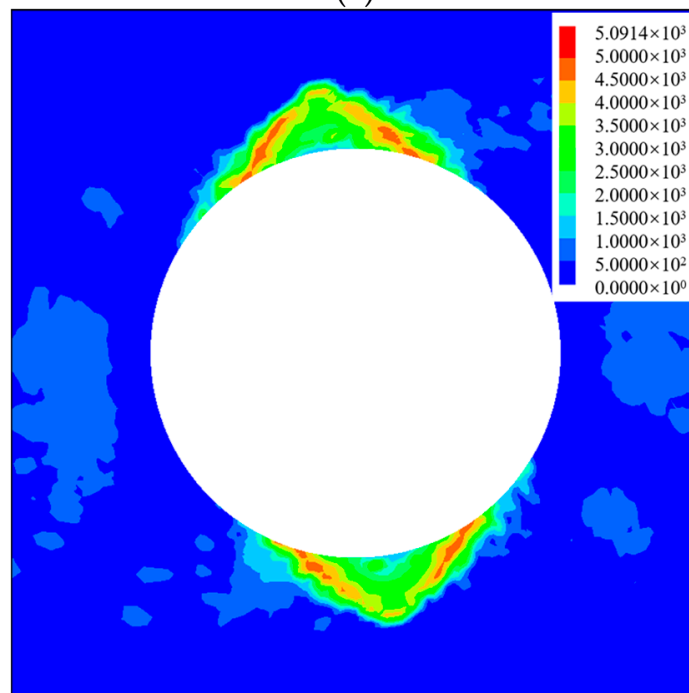


(b)

**Figure 6.** The maximum energy density and its occurrence time before the energy release: (a) maximum energy density; (b) occurrence time of the maximum energy density.



(a)



(b)

**Figure 7.** The energy density and its occurrence time after the energy release: (a) energy density after the energy release; (b) occurrence time of the maximum energy density.

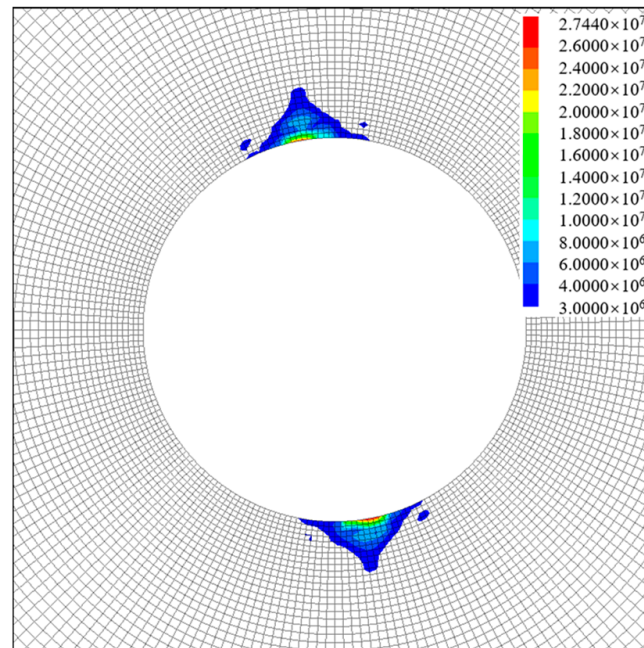


**Figure 8.** Local energy release effectiveness.

## 5. Conclusions

The effectiveness of energy release is greatly influenced by the speed of energy release. To make up for the disadvantage that the existing index fails to consider the time effect of energy release, a stability evaluation index for the excavation of high-stress rock masses considering the speed of energy release was proposed. The validation of the AECL tunnel demonstrated that the index effectively reflected the range and intensity of the dynamic failure of surrounding rocks induced by deep rock mass excavation. Consequently, the index can be used as a reasonable index for stability analysis of high-stress rock mass excavation.

However, the relationship between the energy release effectiveness and energy release speed in the index was defined by referring to the relationship between properties of explosives and fragment size in explosive theory, which may differ from the actual situation to some extent. Furthermore, the index is a relative concept at present. It is necessary to supplement the mechanical test to determine the threshold and modify the relationship between energy release effectiveness and energy release speed.

**Author Contributions:** Conceptualization, S.L. and P.Y.; methodology, W.L. and C.Z.; software, P.Y.; validation, Z.D. and Z.Y.; formal analysis, C.Z.; investigation, S.L.; resources, P.Y.; data curation, S.L.; writing—original draft preparation, S.L.; writing—review and editing, P.Y., W.L., Z.D., Z.Y. and Y.H.; visualization, P.Y.; supervision, W.L.; project administration, P.Y.; funding acquisition, Z.D., Z.Y. All authors have read and agreed to the published version of the manuscript.

**Funding:** This research was funded by the Key Science and Technology Special Program of Yunnan Province (no. 202102AF080001), the Fundamental Research Funds for the Central Public Welfare Research Institutes (CKSF2021462/YT), the Key Science and Technology Special Program of Yunnan Province (no. 202002AF080003), and the National Natural Science Foundation of China (52109148).

**Institutional Review Board Statement:** Not applicable.

**Informed Consent Statement:** Not applicable.

**Data Availability Statement:** The data that support the findings of this study are available from the corresponding author upon reasonable request.

**Acknowledgments:** This work was completed with the contributions of many researchers and their achievements. The authors wish to express thanks to them. To avoid any omission, we express thanks to all supporters.

**Conflicts of Interest:** The authors declare no conflict of interest.

## References

- Zheng, S.R. Discussion on hydropower resources development and environmental & ecological protection in china. *Eng. Sci.* **2006**, *6*, 1–6. [\[CrossRef\]](#)
- Feng, G.L.; Feng, X.T.; Chen, B.R.; Xiao, Y.X.; Liu, G.F.; Zhang, W.; Hu, L. Characteristics of microseismicity during breakthrough in deep tunnels: Case study of Jinping-ii hydropower station in China. *Int. J. Geomech.* **2020**, *20*, 04019163. [\[CrossRef\]](#)
- Zhu, Q.J.; Feng, Y.; Cai, M.; Liu, J.H.; Wang, H.H. Interpretation of the extent of hydraulic fracturing for rockburst prevention using microseismic monitoring. data. *J. Nat. Gas Sci. Eng.* **2017**, *38*, 107–119. [\[CrossRef\]](#)
- Xue, R.; Liang, Z.; Xu, N. Rockburst prediction and analysis of activity characteristics within surrounding rock based on microseismic monitoring and numerical simulation. *Int. J. Rock Mech. Min. Sci.* **2021**, *142*, 104750. [\[CrossRef\]](#)
- Feng, X.T.; Chen, B.R.; Ming, H.J.; Wu, S.Y.; Xiao, Y.X.; Feng, G.L.; Zhou, H.; Qiu, S.L. Evolution law and mechanism of rockbursts in deep tunnels: Immediate rockburst. *CJRME* **2012**, *31*, 433–444. [\[CrossRef\]](#)
- Liang, W.; Sari, Y.A.; Zhao, G.; Mckinnon, S.D.; Wu, H. Probability Estimates of Short-Term Rockburst Risk with Ensemble Classifiers. *Rock Mech. Rock Eng.* **2021**, *54*, 1799–1814. [\[CrossRef\]](#)
- Zhang, J.F.; Wang, Y.H.; Sun, Y.T.; Li, G.C. Strength of ensemble learning in multiclass classification of rockburst intensity. *Int. J. Numer. Anal. Methods Geomech.* **2020**, *44*, 1833–1853. [\[CrossRef\]](#)
- Su, G.S.; Feng, X.T.; Jiang, Q.; Chen, G.Q. Study on new index of local energy release rate for stability analysis and optimal design of underground rockmass engineering with high geostress. *CJRME* **2006**, *25*, 2453–2460. [\[CrossRef\]](#)
- Luo, S. Study on the Mechanism of Influence of Blasting Damage on Rock Burst and Its Control in Deep Tunnel. Ph.D. Thesis, Wuhan University, Wuhan, China, 2021.
- Cook, M.A.; Cook, U.D.; Clay, R.B. Behavior of Rock during Blasting. *Trans. Soc. Min. Eng.* **1966**, *23*, 17–25.
- Carter, J.P.; Booker, J.R. Sudden Excavation of a Long Circular Tunnel in Elastic Ground. *Int. J. Rock Mech. Min. Sci. Geomech. Abstr.* **1990**, *27*, 129–132. [\[CrossRef\]](#)
- Huang, R.Q.; Wang, X.N. Analysis of dynamic disturbance on rock burst. *Bull. Eng. Geol. Environ.* **1998**, *57*, 281–284. [\[CrossRef\]](#)
- Lu, W.B.; Jin, L.; Chen, M.; Zhou, C.B. Study on the mechanism of jointed rock mass loosening induced by dynamic unloading of initial stress during rock blasting. *CJRME* **2005**, *24*, 4653–4657.
- Yi, C.P.; Lu, W.B.; Xu, H.T.; Zhou, C.B. Study on effects of dynamic unloading on initial stress during rock excavation. *CJRME* **2005**, *24*, 4750–4754.
- Lu, W.B.; Chen, M.; Yan, P.; Zhou, C.B. Study on vibration characteristics of surrounding rock induced by tunnel excavation under high in-situ stress. *CJRME* **2007**, *26*, 3329–3334.
- Yan, P. Study on mechanism of the vibration induced by dynamic unloading during rock excavation. *CJRME* **2008**, *27*, 773–781.
- Guo, W.Y.; Tan, Y.L.; Yang, Z.L.; Zhao, T.B.; Hu, S.C. Effect of saturation time on the coal burst liability indexes and its application for rock burst mitigation. *Geotech. Geol. Eng.* **2018**, *36*, 589–597. [\[CrossRef\]](#)
- Di, Y.; Wang, E. Rock burst precursor electromagnetic radiation signal recognition method and early warning application based on recurrent neural networks. *Rock Mech. Rock Eng.* **2021**, *54*, 1449–1461. [\[CrossRef\]](#)
- Sainoki, A.; Mitri, H.S. Numerical investigation into pillar failure induced by time-dependent skin degradation. *Int. J. Min. Sci. Technol.* **2017**, *27*, 591–597. [\[CrossRef\]](#)
- Wang, Y.H.; Chen, L.W.; Shen, F. Numerical modeling of energy release in rockburst. *Rock Soil Mech.* **2008**, *29*, 790–794. [\[CrossRef\]](#)
- Feng, L.F.; Dou, L.M.; Wang, X.D.; Xu, G.G.; Cai, W.; Zhu, G.A.; Jiao, B. Study on influence law of mining speed on stope energy releasing. *Coal Sci. Technol.* **2020**, *48*, 77–84. [\[CrossRef\]](#)
- Fu, J.X.; Song, W.D.; Tan, Y.Y. Criterion of local energy release of gob destabilization in deep mines under unloading stress path. *CJRME* **2016**, *35*, 217–224. [\[CrossRef\]](#)
- Lang, L.; Zhu, Z.; Wang, H.; Huang, J.; Wang, M.; Zhang, X. Effect of loading rates on crack propagating speed, fracture toughness and energy release rate using single-cleavage trapezoidal open specimen under impact loads. *J. Cent. South Univ.* **2020**, *27*, 2440–2454. [\[CrossRef\]](#)
- Compilation Group of Foreign Light Infantry Weapons: Foreign Light Infantry Weapons*; National Defense Industry Press: Beijing, China, 1983.
- Li, X.B.; Gu, D.S. *Rock Impact Dynamic*; Central South University of Technology Press: Changsha, China, 1994.
- Gong, F.Q.; Luo, Y.; Li, X.B.; Si, X.F.; Tao, M. Experimental simulation investigation on rockburst induced by spalling failure in deep circular tunnels. *Tunn. Undergr. Space Technol.* **2018**, *81*, 413–427. [\[CrossRef\]](#)
- Cai, M.; Kaiser, P.K. Assessment of excavation damaged zone using micro mechanics model. *Tunn. Undergr. Space Technol.* **2005**, *20*, 301–310. [\[CrossRef\]](#)

**Disclaimer/Publisher’s Note:** The statements, opinions and data contained in all publications are solely those of the individual author(s) and contributor(s) and not of MDPI and/or the editor(s). MDPI and/or the editor(s) disclaim responsibility for any injury to people or property resulting from any ideas, methods, instructions or products referred to in the content.